Charge-transfer-induced evaporation in collisions of Li$_{31}^{2+}$ clusters with Cs atoms

C. Bréchignac,[1] Ph. Cahuzac,[1] B. Concina,[1] J. Leygnier,[1] L. F. Ruiz,[2] B. Zarour,[3] P. A. Hervieux,[3]
J. Hanssen,[3] M. F. Politis,[4] and F. Martín[2]

[1]*Laboratoire Aimé Cotton, CNRS, Bâtiment 505, Université Paris Sud, 91405 Orsay cedex, France*
[2]*Departamento de Química, C-9, Universidad Autónoma de Madrid, 28049 Madrid, Spain*
[3]*LPMC, Institut de Physique, Technopôle 2000, 57078 Metz, France*
[4]*GPS, Université Paris 7, 2 Place Jussieu, 75251 Paris cedex 05, France*

We present a combined theoretical and experimental study of dissociative charge transfer in collisions of slow Li$_{31}^{2+}$ clusters with Cs atoms. We provide a direct quantitative comparison between theory and experiment and show that good agreement is only found when the experimental time-of-flight and initial cluster temperature are taken into account in the theoretical modeling. This model explains evaporation as resulting from a collisional energy deposit due to cluster electronic excitation during charge transfer. We discuss in detail the basic mechanisms that are responsible for the charge-transfer reaction and different approximations to evaluate the energy deposit.

I. INTRODUCTION

Charge transfer (CT) occurs in numerous physical and chemical processes involving atomic, molecular, or biological species and surfaces. The fundamental aspects of CT have been thoroughly investigated in atomic and molecular systems since the early days of quantum mechanics, while surfaces have been considered more recently in connection with technological applications. The study of CT with clusters has received much less attention.

The available experimental techniques allow one to selectively prepare metal clusters of almost any size. Thus metal clusters are the ideal tool to bridge the gap between molecules and surfaces. A singular aspect of CT in cluster-atom collisions is that it competes with electron excitation and dissociation even at low impact energies [1–3]. This makes experiments difficult to analyze and it is also a challenge for theoretical models which, among the large number of electronic and nuclear degrees of freedom, have to uncover the most relevant ones for the physics of the problem (see, e.g., Refs. [2,4–7] and references therein). As a consequence, rigorous attempts to confront theory and experiment at a quantitative level are very scarce. Among them, the study of CT in Na$_9^+$ + Cs collisions has played a very important role [8–12] because this is the first system for which the theory [11] has been able to provide absolute CT cross sections in good agreement with experiment [8].

Nevertheless, the sole study of CT is not enough for a complete description of the collision dynamics. To understand the complexity of the latter, one must consider that, after CT, most clusters evaporate one or several fragments. This fact must be taken into account for a direct comparison between theory and the experimental observables, namely the relative intensities of the cluster fragments. As recent theoretical work on Na$_9^+$ + Cs [12] has shown, this comparison is not straightforward. The latter work has shown that evaporation cross sections critically depend on the initial temperature of the cluster T_0 and the experimental time-of-

flight (TOF) window τ_e. While the TOF can be accurately determined in most experiments, the initial temperature of the cluster is only known indirectly. In fact, temperature is evenly distributed in a finite interval [13,14] which, for small Li and Na clusters, may be as large as 200–1200 K.

In a recent paper [15], we have reported a combined experimental and theoretical study of collisions of slow Li$_{31}^{2+}$ clusters with Cs atoms. Li$_{31}^{2+}$ clusters lie slightly above the appearance size of doubly charged clusters, which implies that the fission channel is barely important and clusters dissociate by evaporating neutral fragments (monomers and traces of dimers). For this collision system, the experimental conditions can be strictly controlled. In the first place because lithium clusters are among the best known clusters. More importantly, CT products resulting from the collision are singly charged cluster ions, which can be easily detected and mass analyzed by TOF spectrometry. This is in contrast with Na$_9^+$ + Cs collisions for which CT leads to neutral species that are difficult to analyze (actually mass spectrometry of laser photoionized neutral fragments has been performed [1], but even when threshold ionization conditions are satisfied, fragmentation due to ionization itself cannot be totally ruled out). In addition, Li$_{31}^{2+}$ clusters can be produced quite abundantly [16] and, as other doubly charged cluster containing an odd number of atoms, can be unambiguously mass selected. This implies higher peak intensities in the measured spectrum. Finally, Li$_{31}^{2+}$ clusters are produced as an "evaporative ensemble" with a relatively narrow temperature distribution, $420 \pm 50 - 660 \pm 50$ K, which allows one to better analyze the role played by the initial internal energy of the cluster in the evaporation process.

This has allowed us to obtain a much deeper insight on the relation between CT and evaporation than previously reported. In particular, we have proved [15] the validity of the simple physical image that consists in explaining evaporation as resulting from a collisional energy deposit due to cluster electronic excitation during the CT process. This is justified by the different time scales associated with CT and evapora-

tion. Our results have shown that theory only agrees with experiment when the experimental time of flight ($\tau_e = 4.5$ μs) and initial cluster temperature are used in the theoretical modeling. When the evaporation process is treated separately from the collision dynamics, accounting for the TOF is a very simple matter. However, when CT and evaporation are treated on an equal footing, as in molecular dynamics simulations [2], integration of the resulting equations is so time consuming that it is practically impossible to reach the values of the TOF in a typical experiment. In Ref. [15] we have also analyzed the influence of initial cluster temperature by assuming that all clusters have the same value of T_0. Nevertheless, as we will see below, Li_{31}^{2+} clusters are produced as an evaporative ensemble, which means that one has to use a temperature distribution instead of a single value of T_0.

In this paper we discuss several aspects that have been omitted in Ref. [15]. The first one is the mechanism that leads to CT in $Li_{31}^{2+} + Cs$ collisions. This will be done with the help of energy correlation diagrams and inclusive probabilities similar to those used to analyze CT in ion-atom collisions. We also analyze in detail the origin of the energy deposit that is responsible for the observed fragmentation pattern. The energy deposit is the link between CT and evaporation. It arises naturally as an intermediate step in the theoretical model and, although it is not an observable in the experiment, we will also discuss an approximate method to estimate its average value from the observed fragmentation ratios. This procedure can be very useful to obtain information about the primary CT process when a complete theoretical description is not possible. Finally, we analyze the role of initial temperature by using an initial energy distribution compatible with the evaporative ensemble produced in the experiment.

In Sec. II, we describe the experimental apparatus. From the measurements, we deduce the expected temperature distribution of the cluster projectiles (Sec. III). In Sec. IV, we present the energy correlation diagrams and calculated CT probabilities. Comparison between measured and calculated evaporation cross sections is presented in Sec. V. We end with some conclusions in Sec. VI. Atomic units are used in the theoretical sections, unless otherwise stated.

II. EXPERIMENT

A. Experimental setup

We start by briefly describing the experimental apparatus (a detailed presentation can be found in Refs. [1,13,16]). A distribution of lithium neutral clusters is generated by a gas aggregation source. They are ionized within the multigrid acceleration device of a tandem Wiley-Mc-Laren TOF mass spectrometer by a 10 ns pulsed KrF eximer laser at a photon energy of 5 eV (Fig. 1). The laser intensity is large enough to (multi)ionize, photoexcite, and warm the clusters during the 10 ns pulse duration. Rapid sequential evaporation occurs during the residence time in the ionizing region (the residence time is the propagation time of ionized clusters into the multigrid ionization/acceleration device and is $\simeq 1$ μs). This shifts down to lower masses the initial cluster distribu-
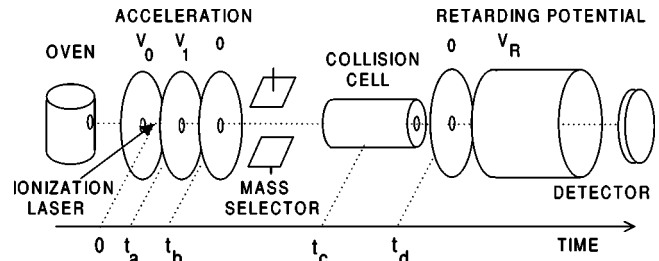

FIG. 1. Experimental setup. Li_{31}^{2+} clusters are mass selected, then interact with a gas of Cs atoms. The collision products are charge and mass analyzed at t_d by a retarding potential method.

tion. Under these conditions, clusters entering the TOF constitute an evaporative ensemble [14] with a temperature distribution that depends on the experimental time windows. The ion kinetic energy is determined by the accelerating voltage V_0, which is varied from 2 to 8 kV. In the first drift tube of the TOF the clusters are selected by an electrostatic gate according to their mass/charge ratio, and then cross a 20-cm-long collision cell containing (or not) the target. The active part of the cell is ~ 10 cm (from now on we will refer to the latter value of the distance whenever the collision cell is mentioned). The cell pressure is maintained low enough to ensure single-collision conditions. Downstream the cell, but upstream the second drift tube, a retarding electrostatic potential V_R allows to separate in time charged products and neutral packets.

Clusters produced as an evaporative ensemble contain a certain amount of internal energy. Thus, they partially undergo unimolecular dissociation (UD) during their propagation in the TOF. Under our experimental conditions and for the relevant cluster sizes, UD is dominated by evaporation of a neutral monomer:

$$Li_{31}^{2+} \rightarrow Li_{30}^{2+} + Li. \tag{1}$$

The dissociation ratio $Li_{30}^{2+}/Li_{31}^{2+}$ depends on the two time windows of the experiment: the residence time in the accelerating region ($t_b \sim 2$ μs) and the propagation time in the first drift tube ($t_d - t_b \sim 19 \pm 0.4$ μs). The products from the UD process propagate in the first drift tube with the center-of-mass velocity of the parent. They are spatially resolved into individual mass packets in the second drift tube thanks to the retarding potential. They are observed even when the cesium pressure in the collision cell is extremely low (smaller than 10^{-6} torr). When the cell is activated, the structure displayed by the retarding field images the combined effects of the UD and charge-exchange processes. Thus, by comparing the spectra obtained cell on and cell off, one identifies the signals that are exclusively due to CT.

B. Measurements

Figure 2 shows mass spectra corresponding to three values of the retarding potential $V_R = 0$, 1250, and 2500 V. The atomic density in the cell is $\simeq 2 \times 10^{11}$ atoms/cm^3. When the potential is switched off the ion peak contains the residual parent and all the collision products. At the intermediate V_R
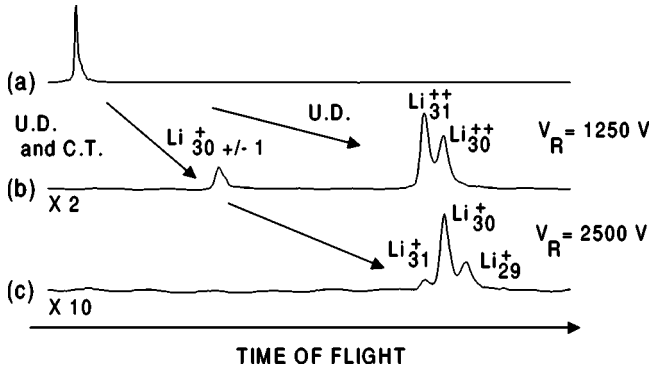
FIG. 2. Li_{31}^{2+} clusters are isolated in the first part of a time-of-flight spectrometer, then collide with a gas of Cs atoms (single-collision conditions). With no applied retarding potential, all the unimolecular decay and collisional products form a single TOF mass peak (a). In parts (b) and (c), a retarding potential of 1250 and 2500 V, respectively, disperse UD and collisional products following their charge/mass ratio.

value, one distinguishes, for increasing values of the TOF, a shouldered peak whose center of mass corresponds to the singly charged species Li_{30}^+, and a twinned structure which includes the residual Li_{31}^{2+} parent and the Li_{30}^{2+} fragment. The intensity of the shouldered peak varies with the cell pressure and, therefore, it is associated with the singly charged species that are directly produced by CT. In contrast, the relative intensity of the twinned peaks is not sensitive to the cell pressure and so remains for vanishingly low values of the cell pressure. Thus Li_{30}^{2+} clusters are the products of the Li_{31}^{2+} unimolecular decay that occurs between t_b and t_d and, consequently, the twinned peaks are unambiguously associated with the UD process (1) and not to a collisional-induced dissociation process which should lead to a signal proportional to the atomic vapor density. This is further confirmed by the fact that the $Li_{31}^{2+}/Li_{30}^{2+}$ ratio observed in Fig. 2 is practically the same as when the collision cell is inactive.

The increase of V_R increases the mass discrimination and reveals a structure within the singly charged mass peak. It appears now as a distribution of three components identified as Li_{29}^+, Li_{30}^+ and Li_{31}^+, Li_{30}^+ being the dominant structure. Li_{31}^+ clusters can only arise from CT, while Li_{30}^+ clusters can arise either from monomer evaporation following CT to Li_{31}^{2+} or directly from CT to Li_{30}^{2+}; similarly, Li_{29}^+ clusters can arise from evaporation following CT to either Li_{31}^{2+} or Li_{30}^{2+}. Since there is more fragmentation for the singly charged species than for the doubly charged species, the evaporation rate associated with the former must be much larger than for the latter [see Eq. (1)]. Moreover, the former involves a relatively short propagating time, from the collision cell up to the retarding potential plate, which leads us to conclude that CT is accompanied by a significant amount of energy deposit in the cluster ion. As we will see later, this energy deposit involves cluster excited states.

Summarizing the observations, the following channels are relevant to deduce the cross sections: (i) CT occurring for both the parent and its UD products entering the collision cell [see Eq. (1)]:

$$Li_{31}^{2+} + Cs \rightarrow Li_{31}^+ + Cs^+, \qquad (2)$$

$$Li_{30}^{2+} + Cs \rightarrow Li_{30}^+ + Cs^+; \qquad (3)$$
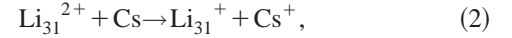
(ii) evaporation of excited singly charged products (the absence of Li_{28}^+ clusters gives a limit to the sequences):

$$Li_{31}^+ \rightarrow Li_{30}^+ + Li \rightarrow Li_{29}^+ + 2Li, \qquad (4)$$

$$Li_{30}^+ \rightarrow Li_{29}^+ + Li. \qquad (5)$$
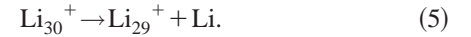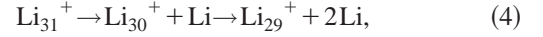
C. CT cross sections

As shown in Ref. [8], CT cross sections for medium-size singly charged Li clusters barely depend on cluster size. Therefore, it is reasonable to assume that the cross sections associated with Eqs. (2) and (3) are identical. Thus, we can easily deduce the absolute value of the CT cross section σ from Beer's law:

$$1 - \frac{[Li_{31}^+] + [Li_{30}^+] + [Li_{29}^+]}{[Li_{31}^{2+}]^0 + [Li_{30}^{2+}]^0} = \exp(-\sigma n_{at} l), \qquad (6)$$

where the denominator contains the area of the parent ion signal before the collision and the numerator the area of the signal associated with the charge-exchange products. n_{at} is the atomic vapor density and l is the length of the collision cell. In order to overcome the uncertainty on the $n_{at} l$ value, we have also used Li^+ projectiles and have compared our values with the absolute cross sections of Perel and Daley for the same collisional system and collision energy [17]. From this comparison, we have renormalized our results for the $Li_{31}^{2+} + Cs$ collision. We have found for the latter $\sigma = 250 \pm 50\,\text{Å}^2$ for an impact energy of 3 keV. The main part of the uncertainty comes from the differences in the focusing conditions of singly doubly charged species and of the various sizes of the fragments. We have minimized these effects by using appropriate values of the retarding potential. The final uncertainty is essentially the sum of this contribution and the uncertainty due to the calibration procedure. We have checked that, within the experimental uncertainty, the CT cross section barely changes in the energy range 1–8 keV (laboratory frame). Similar results have been found for the magnitude and the variation of the CT cross section with collision energy in the case of K targets. Previous measurements with doubly charged Na clusters led to comparable results, with a slow decrease of the cross section with the collision energy [18]. These values are remarkably larger than those found for singly charged species with the same number of atoms and at the same collisional energy [18].

III. MODELING THE EXPERIMENTAL CONDITIONS

A. Initial energy distribution

When the collision cell is off, one only observes UD [see Eq. (1)], hence it is possible to deduce the internal energy

(temperature) distribution of Li_{31}^{2+} and Li_{30}^{2+} projectiles before CT occurs. This can be done by using the evaporative ensemble model in the framework of the statistical Weisskopf theory (see Ref. [16] and Sec. IV B). In this work we have improved this model by including anharmonic effects for the evaluation of the evaporation rate constants.

Li_N^{2+} clusters accelerated at t_a result from a long sequence of evaporation events following the large neutral cluster photoionization and photofragmentation ($t=0$). As the last evaporation step is much longer than the previous ones, this evaporation chain can be written as

$$\cdots \rightarrow Li_{N+1}^{2+}(E_{N+1}^*, t=0) \overset{k_{N+1}}{\rightarrow} Li_N^{2+}(E_N^*, t=t_a) \overset{k_N}{\rightarrow} \cdots, \tag{7}$$
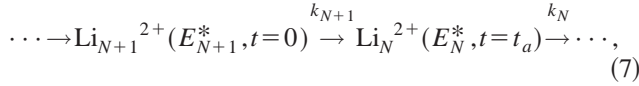
where E_{N+1}^*, E_N^*, k_{N+1}, and k_N are the internal energies and the evaporation rate constants, respectively, for Li_{N+1}^{2+} and Li_N^{2+}, respectively. The evaporation rates have been evaluated as explained in Sec. IV B below.

For a cluster Li_{N+1}^{2+} containing an internal energy E_{N+1}^* at $t=0$, the probability to form Li_N^{2+} at $t=t_a$ by evaporation is

$$k_{N+1}\left(\frac{\exp[-k_{N+1}t_a]}{k_N-k_{N+1}} + \frac{\exp[-k_N t_a]}{k_{N+1}-k_N}\right).$$

The experimental conditions are such that all values of E_{N+1}^* are equally probable in the energy domain of interest. Consequently, the distribution of internal energy for an ensemble of clusters Li_N^{2+} mass dispersed at $t=t_a$ is given by

$$\mathcal{D}_N^{(a)}(E^*) = k_{N+1}\left(\frac{\exp[-k_{N+1}t_a]}{k_N-k_{N+1}} + \frac{\exp[-k_N t_a]}{k_{N+1}-k_N}\right). \tag{8}$$

To simplify the notation, the dependence of k_{N+1} and k_N with the cluster internal energy has not been indicated. The clusters appearing in the TOF mass spectra peaks are those that do not evaporate during the acceleration time $t_b - t_a$. For a packet of Li_N^{2+} clusters accelerated at t_a and surviving until t_b, the internal energy distribution is

$$\mathcal{D}_N^{(b)}(E^*) = \mathcal{D}_N^{(a)}(E^*)\exp[-k_N(t_b-t_a)]. \tag{9}$$

This distribution is shown in Fig. 3(a). If the collision cell is kept inactive, the mass-selected Li_N^{2+} packet evolves only by unimolecular decay. As only one evaporation step is observed, the evaporation fraction for the unimolecular decay taking place in the field-free part of the TOF mass spectrometer (time interval $[t_b, t_d]$) can be written as

$$F_N = \frac{\int \mathcal{D}_N^{(b)}(E^*)\{1-\exp[-k_N(t_d-t_b)]\}dE^*}{\int \mathcal{D}_N^{(b)}(E^*)dE^*}. \tag{10}$$

The value calculated for $N=31$ is in good agreement with the measured one. The internal energy of Li_N^{2+} ions at t_c,
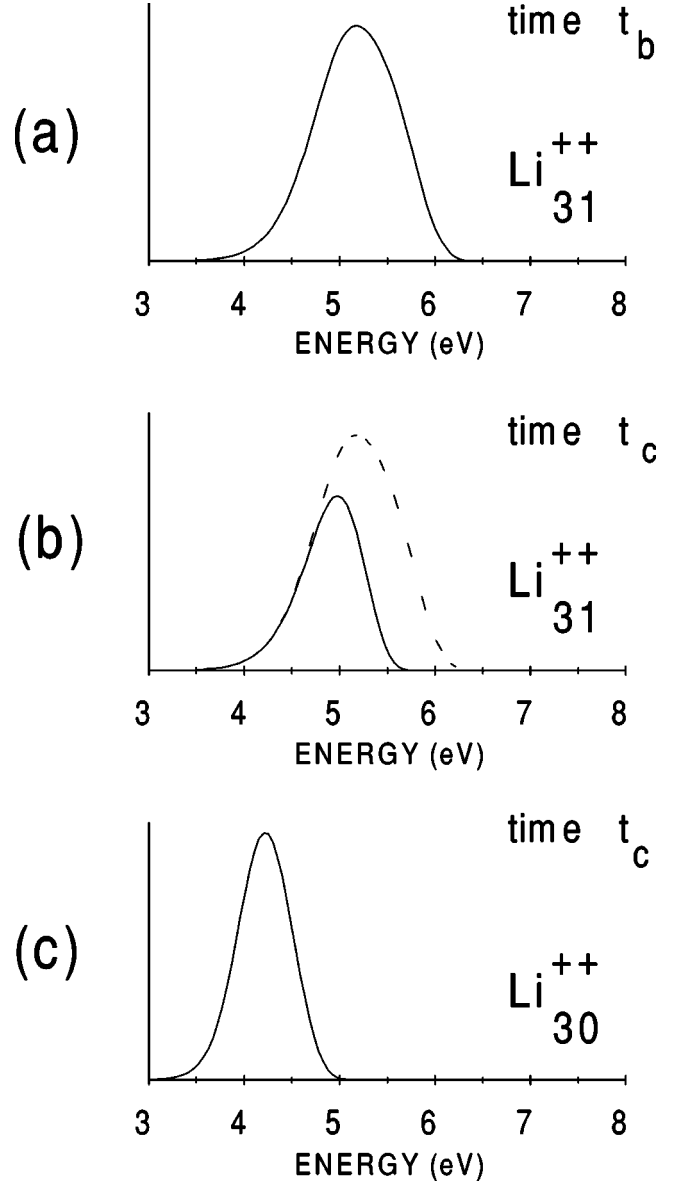

FIG. 3. Internal energy distribution for a packet of (a) Li_{31}^{2+} clusters dispersed at time t_b (entrance of the field-free part of the TOF), (b) intact Li_{31}^{2+} clusters entering the collision cell at t_c, and (c) Li_{30}^{2+} clusters entering the collision cell that were formed by evaporation between t_b and t_c.

i.e., of those clusters for which there is no unimolecular decay between t_b and t_c, is given by

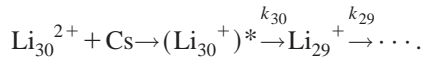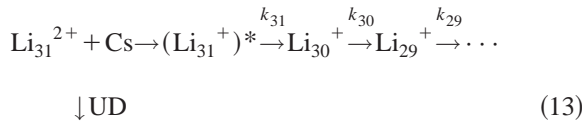$$\mathcal{D}_N^{(c)}(E^*) = \mathcal{D}_N^{(b)}(E^*)\exp[-k_N(t_c-t_b)]. \tag{11}$$

The latter energy distribution is shown in Fig. 3(b). Those warm enough to evaporate before t_c produce Li_{N-1}^{2+}. The energy balance is $E_{N-1}^* = E_N^* - D_N - \epsilon$, where D_N is the parent cluster dissociation energy and ϵ the kinetic energy released in the evaporation reaction. For all the Li_{N-1}^{2+} evaporation products obtained in the experimental conditions, the internal energy distribution is then

$$\mathcal{D}_{frag}^{(c)}(E^*) = \mathcal{D}_N^{(b)}(E^* + D_N + \epsilon)\{1 - \exp[-k_N(t_c - t_b)]\}.$$

$$(12)$$

This distribution is given in Fig. 3(c). Equations (11) and (12) define the mass and internal energy distributions for the packet of doubly charged lithium clusters interacting with cesium atoms in the experimental conditions.

B. Collisional energy deposit

From the fragmentation patterns observed when the cell is on, we can also estimate the internal energy of the singly charged clusters formed in the collision. Due to unimolecular decay, the cluster packet entering the collision cell contains $\approx 58\%$ Li_{31}^{2+} and 42% Li_{30}^{2+} [see Figs. 2(b), 3(b), and 3(c)]. As will be discussed in Sec. IV, the collision of these two species with the Cs target leads to singly charged clusters in an electronic excited state. This excitation energy (or energy deposit) is responsible for the sequence of evaporation events that take place in the time interval $[t_c, t_d]$ between the collision and the electrostatic analysis of the collision fragments:

$$Li_{31}^{2+} + Cs \rightarrow (Li_{31}^+)^* \xrightarrow{k_{31}} Li_{30}^+ \xrightarrow{k_{30}} Li_{29}^+ \xrightarrow{k_{29}} \cdots$$

$$\downarrow UD \qquad\qquad (13)$$

$$Li_{30}^{2+} + Cs \rightarrow (Li_{30}^+)^* \xrightarrow{k_{30}} Li_{29}^+ \xrightarrow{k_{29}} \cdots .$$

We define $P_{31-p}^{31}(E^*, \tau_e)$ and $P_{30-p}^{30}(E^*, \tau_e)$ the probabilities to form Li_{31-p}^+ (Li_{30-p}^+) clusters after an evaporation time $\tau_e = t_d - t_c$ from a Li_{31}^+ (Li_{30}^+) parent with internal energy E^* after the collision. These probabilities are obtained following a procedure similar to that explained in the preceding section. Thus, for example, we can write $P_{31}^{31}(E^*, \tau_e) = \exp[-k_{31}\tau_e]$ and

$$P_{31-p}^{31}(E^*, \tau_e) = \prod_{i=0}^{p-1} k_{31-i} \sum_{\ell=0}^{p} \frac{\exp[-k_{31-\ell}\tau_e]}{\displaystyle\prod_{j=0, j \neq \ell}^{p} (k_{31-j} - k_{31-\ell})}.$$

$$(14)$$

Figure 4 shows the probabilities P_{28}^{31} and P_{28}^{30} as functions of the internal energy E^* contained in the parent clusters immediately after the collision (notice that E^* contains both the initial cluster energy and the collision energy deposit). The results of Fig. 2 show that no Li_{28}^+ fragments are observed in the experiment (strictly speaking, these fragments cannot be observed when they represent typically less than 5% of the total fragmentation signal). Now, we can combine this result with the probabilities shown in Fig. 4 to estimate an experimental upper bound to the collisional energy deposit. The latter figure shows that, within the 5% uncertainty, Li_{28}^+ fragments are not observed when Li_{31}^+ and Li_{30}^+ clusters resulting from CT contain, respectively, an internal energy smaller than 7.4 and 6.1 eV after the collision. Taking into account that the initial internal energy distributions of
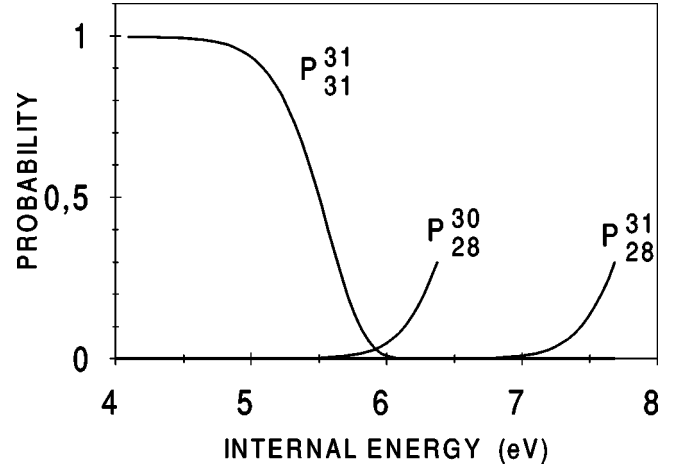
FIG. 4. Probabilities $P_{N-p}^N(E^*, \tau_e)$ to obtain Li_{N-p}^+ from Li_N^{2+} after an evaporation time $\tau_e = t_d - t_c = 4.5$ μs. The evaporation time is fixed by the experimental setup.

Li_{31}^{2+} and Li_{30}^{2+} clusters entering the collision cell are centered around 5.0 and 4.2 eV, respectively (see Figs. 3(b,c)], one infers that the collision energy deposit must be smaller than 2.4 eV for Li_{31}^+ and smaller than 1.9 eV for Li_{30}^+. This leads to an upper bound of 1.9 eV. This value is compatible with the average value of 1.0 ± 0.1 estimated in Ref. [15].

IV. THEORY

In addition to the experiment described in the previous sections, we have carried out theoretical calculations using the method of Refs. [7,12]. This method has been previously used to study CT and fragmentation in $Na_9^+ + Cs$ collisions. The method benefits from the different time scales associated with the collision and the internal motion of the cluster nuclei. In the first place, because the collision time ($\tau_{col} \sim 10^{-14}$ s) is much shorter than the cluster vibrational period ($\tau_v \sim 10^{-12}$ s) in the range of impact velocities considered in this work ($v \sim 0.01$–0.03 a.u. or 1–4 keV). In the second place, because clusters that are electronically excited during the collision relax their excess energy once the collision is over (the electron-phonon coupling responsible for the observed dissociation has a characteristic lifetime of $\tau_{rel} \sim 10^{-13}$–10^{-12} s and, therefore, can be ignored during the collision). As a consequence, the only nuclear degree of freedom that is relevant in the CT dynamics is the relative distance R between the impinging cluster and the atomic target. Furthermore, evaporation is a postcollisional effect that can be described separately provided that the collisional energy deposit δE and the initial cluster temperature are known. Still, dissociation may be induced in frontal collisions with the target, but this will not be taken into account because the present experimental results show that it is a minor dissociation channel (a similar situation can be found in Refs. [10,16]). This is consistent with the fact that evaporation induced by CT occurs at long distances and, therefore, is the dominant process.

According to the above discussion, the collision and the

subsequent evaporation process have been treated separately, being δE the connection between these two problems.

A. Collision dynamics

The collision is studied using a fully quantum-mechanical description of the relevant electronic degrees of freedom in the framework of the independent electron model. Since, this part of the theory has been described in detail in Ref. [7], here we only summarize the basic ingredients. We represent the Cs atom as a one-electron system in which the xenonlike core is replaced by a local model potential that approximately reproduces the Hartree-Fock potential felt by the $6s$ valence electron [19]. A major simplification is the use of the spherical jellium model to represent the ionic core potential of the cluster. In this model, the real potential is replaced by a constant positive background of radius $R_C = 10.2$ a.u. This is known to be a good approximation for large closed-shell metal clusters [20] but requires a more careful justification for an open-shell metal cluster such as Li_{31}^{2+}. To our knowledge, the geometry of lithium clusters containing more than 20 atoms is not known. In contrast, sodium clusters are much better known and one can expect them to behave in a similar way. In this respect, Calvo and Spiegelmann [21,22] have predicted that sodium clusters (with more than 20 atoms) undergo permutational isomerization between topologically identical forms at relatively low temperatures (of the order of 200 K). This spontaneous isomerization is due to the great mobility of the sodium atoms and implies that the clusters are in a liquid phase. Thus, above 200 K, the spherical jellium approximation provides, on average, a more realistic picture of the cluster than that corresponding to the lowest-energy geometry. Since in the present experimental conditions the cluster temperature lies in the interval 420–660 K, the spherical jellium model is expected to provide a correct average description of Li_{31}^{2+}.

In this context, we have applied the Kohn-Sham formulation of density-functional theory to describe the cluster electron density in terms of single-particle orbitals. Then, from these orbitals, we have obtained the corresponding one-electron potentials using a local-density approximation with exchange, correlation, and a self-interaction correction (LDAXC-SIC, see Ref. [7] for details). Introduction of the self-interaction correction leads to orbital-dependent potentials with the correct asymptotic behavior, which is crucial in the present study because capture and excitation processes occur mainly at large distances.

As a consequence of the quasiseparability of the cluster Hamiltonian, the total N_e-electron Hamiltonian $\hat{\mathcal{H}}$ (where N_e includes the 29 valence electrons of Li_{31}^{2+} and the valence electron of Cs) has been written as a sum of one-electron effective Hamiltonians, $\hat{\mathcal{H}} = \Sigma_{i=1}^{N_e} \hat{h}(i)$, with

$$\hat{h} = -\frac{1}{2}\nabla^2 + V_{Cs^+}(|\mathbf{r}-\mathbf{R}|) + V_C(\mathbf{r}), \quad (15)$$

where V_{Cs^+} is the model potential representing the Cs^+ ion, and V_C is the cluster potential; notice that the origin of electronic coordinates has been placed on the cluster center and

that $\mathbf{R}$ is the Cs position vector. The cluster potential V_C has been obtained from the orbital-dependent LDAXC-SIC potentials using the global average scheme proposed in Ref. [7]. This has been shown to be accurate enough for the description of static and dynamic properties, even in a strong excitation regime [23]. Thus, the N_e-body dynamical treatment reduces to a set of N_e one-electron problems. The latter are treated in the framework of the impact-parameter method, where the projectile follows a straight-line trajectory and the electron is described quantum mechanically. Assuming that each electron i is initially in a $\phi_i(\mathbf{r})$ spin orbital of energy ϵ_i, one has to solve a set of N_e time-dependent Schrödinger equations

$$\hat{h}\psi_i(\mathbf{r},t) = i\frac{d}{dt}\psi_i(\mathbf{r},t), \quad i=1,\ldots,N_e, \quad (16)$$

where each $\psi_i(\mathbf{r},t)$ is subject to the initial condition

$$\lim_{t\to-\infty}\psi_i(\mathbf{r},t) \to \phi_i(\mathbf{r})\exp[-i\epsilon_i t]. \quad (17)$$

The collision velocities considered in this work are much smaller than the orbital velocities of the cluster electrons near the Fermi level and the orbital velocity of the Cs valence electron. Thus, Eq. (16) has been solved by expanding the one-electron wave functions in a basis of Born-Oppenheimer (BO) *molecular* states $\{\chi_k(\mathbf{r},R)\}$. These states have been obtained by diagonalizing $\hat{h}$ in a two-center *atomic* basis built from spherical Gaussian-type orbitals with angular momentum up to $l=6$. Figure 5 shows the BO potential-energy curves for the σ states of the $(Li_{31}\text{-}Cs)^{2+}$ *quasimolecule*. The initially occupied orbitals are $1s$, $1p$, $1d$, $2s$, and $1f$ for Li_{31}^{2+} and $6s$ for Cs (for simplicity, we use the "separate atom" notation to refer to molecular orbitals). The asymptotically occupied $6s$ orbital of Cs mainly interacts with the $2f$, $3p$, $1h$, and $3s$ orbitals of Li_{31}^{2+}, which are initially empty. The corresponding radial couplings are shown in Fig. 6. It can be seen that the $Cs(6s)$ state presents avoided crossings with the $2f$, $3p$, $1h$, and $3s$ ones of Li_{31}^{2+} at $R \simeq 30$ a.u. and, consequently, the corresponding radial couplings exhibit sharp maxima in that region. Since the $6s$ orbital of Cs has $m=0$ (it is a σ orbital), electron transfer to cluster orbitals with $m\neq 0$ is only possible through rotational couplings. As the latter are only relevant at small R, they do not play a significant role in the charge-transfer reaction. Thus, we have limited the expansion of ψ_i to molecular states of σ symmetry. More precisely, we have expanded ψ_i in the basis of 20 states shown in Fig. 5, which includes the $6s$ and $6p$ states of Cs, the $1s$, $1p$, $1d$, $2s$, and $1f$ states dissociating into occupied cluster orbitals, and 14 states dissociating into unoccupied cluster orbitals, namely $2p$, $1g$, $3s$, $2d$, $1h$, $3p$, $2f$, etc. This set of states allows one to describe charge transfer as well as cluster excitations.

The inclusive probability $P_{f_1,\ldots,f_q}$ of finding q of the N_e electrons in the subconfiguration $(f_1,\ldots,f_q)$ while the remaining N_e-q ones occupy any other states after the collision is given by the $(q\times q)$ determinant [24]
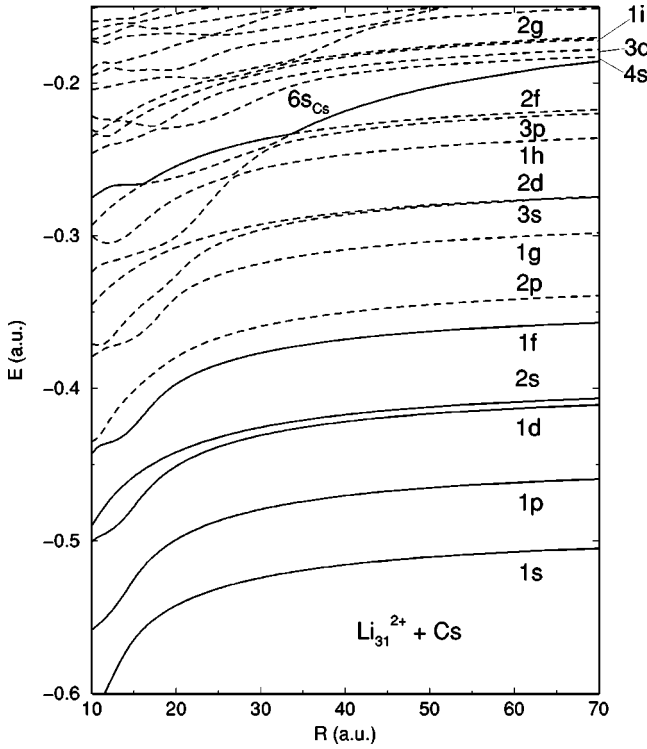
FIG. 5. Energy correlation diagram for the σ *molecular* orbitals (MOs) of the $(Li_{31}-Cs)^{2+}$ *quasimolecule*. R denotes the distance of the Cs atom to the cluster center. Labels nl and nl_{Cs} denote, respectively, the cluster and the Cs orbitals to which the MOs correlate at $R=\infty$. Full lines, initially occupied orbitals; dashed lines, initially unoccupied orbitals. Notice that the avoided crossings between the Cs(6s) state and the $4s$, $3d$, and higher states have been replaced by crossings because they occur at $R>70$ a.u. and, therefore, are transversed diabatically at the collision energies considered in this work.
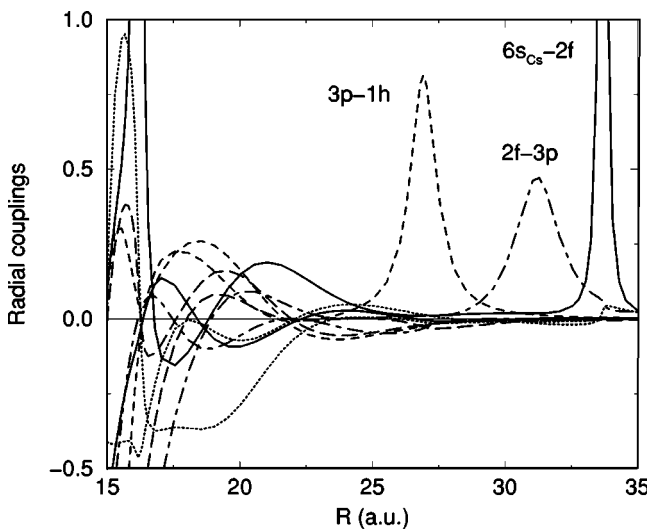

FIG. 6. Radial couplings between the σ MOs of the $(Li_{31}-Cs)^{2+}$ quasimolecule. Only couplings between the $6s_{Cs}$, $2f$, $3p$, $1h$ and $2d$ states are shown (see Fig. 5). R denotes the distance of the Cs atom to the cluster center.

$$P_{f_1,\ldots,f_q} = \det(\gamma_{nn'}), \quad n,n'=1,\ldots,q, \quad q<N_e, \tag{18}$$

where $\gamma_{nn'}$ is the one-particle density matrix built from the one-electron transition amplitudes. The inclusive probability of finding q occupancies and $L-q$ holes, $P_{f_1,\ldots,f_q}^{f_{q+1},\cdots,f_L}$, can be written in terms of probabilities (18) related only to occupancies. The explicit equations can be found in Ref. [24]. In this work we have evaluated the inclusive probabilities:

$$P^{6s\overline{6s}6p\overline{6p}\cdots} \quad \text{and} \quad P_j^{6s\overline{6s}6p\overline{6p}\cdots}, \tag{19}$$

which represent, respectively, the probability of finding no electrons in the Cs valence orbitals $(6s,6p,\cdots)$ and the probability that, simultaneously, an electron is in the j excited orbital of the Li_{31}^+ cluster. In this work j runs over the following cluster orbitals: $2p$, $1g$, $3s$, $2d$, $1h$, $3p$, $2f$, $4s$, $3d$, $1i$, $2g$, etc. (remember that $1f$ is the highest occupied orbital of Li_{31}^+). $P^{6s\overline{6s}6p\overline{6p}\cdots}$ is, therefore, the probability of finding Cs^+ ions after the collision. The Cs^+ ions can be formed through charge transfer or ionization, but since Cs ionization is negligible at the impact energies considered in this work, $P^{6s\overline{6s}6p\overline{6p}\cdots}$ can be interpreted as a charge-transfer probability. $P^{6s\overline{6s}6p\overline{6p}\cdots}$ must be evaluated by including all the Cs orbitals used in the close-coupling expansion, i.e., $6s$, $\overline{6s}$, $6p$, and $\overline{6p}$ in the present case.

The excitation energy of the Li_{31}^+ clusters produced by CT, $E_{Li_{31}^+}^*$, is given by

$$E_{Li_{31}^+}^*(b) = \delta E_{Li_{31}^+}(b) + E_0^*, \tag{20}$$

where E_0^* is the initial vibrational energy of the Li_{31}^{2+} cluster before the collision and $\delta E_{Li_{31}^+}$ is its electronic excitation energy due to CT. The latter is given by

$$\delta E_{Li_{31}^+}(b) = \sum_k (E_k - E_g) P_{f_{1_k}\cdots f_{N_{e_k}}}(b), \tag{21}$$

where the sum on k runs over all possible configurations built by including all 30 active electrons in Li_{31}^+ orbitals (i.e., no valence electron in the Cs nucleus), E_k is the energy of the Li_{31}^+ cluster in the k configuration:

$$E_k = \sum_{j=1}^{N_e} \epsilon_{j_k} \tag{22}$$

and E_g is the ground-state energy of Li_{31}^+. The sum in Eq. (21) includes, in general, a huge number of exclusive probabilities that are difficult to evaluate in practice. For this reason, we have used two approximate formulas. The first one is given by

$$\delta E_{Li_{31}^+}(b) = \sum_j \Delta\epsilon_j P_j^{6s\overline{6s}6p\overline{6p}\cdots}(b), \tag{23}$$

where $\Delta\epsilon_j = \epsilon_j - \epsilon_{1f}$. This formula is obtained from Eq. (21) by assuming that all cluster configurations containing an

electron in an excited j orbital are associated with the same excitation energy $\Delta\epsilon_j$, i.e., they are associated with a single-electron process in which the cluster has captured the Cs electron in the j orbital and the other cluster electrons remain as spectators. Thus Eq. (23) does not include information on all those multiple processes in which charge-transfer and inner-shell vacancies are produced simultaneously. Therefore, it is a lower bound to the exact collisional excitation energy.

The second formula is given by

$$\delta E_{\mathrm{Li_{31}}^+}(b) = \langle \Psi_{f_1, \ldots, f_{N_e}} | \hat{\mathcal{H}} - E_g | \Psi_{f_1, \ldots, f_{N_e}} \rangle, \quad (24)$$

where $\Psi_{f_1, \ldots, f_{N_e}}$ is the N_e-electron wave function that results from solving the time-dependent Schrödinger equation up to $t = +\infty$, i.e., it is the Slater determinant $\Psi_{f_1, \ldots, f_{N_e}} = \| \psi_{f_1} \cdots \psi_{f_{N_e}} \|$ at $t = +\infty$. Equation (24) can be written in terms of inclusive probabilities

$$\delta E_{\mathrm{Li_{31}}^+}(b) = \sum_j P_j \Delta\epsilon_j = \sum_j \gamma_{jj} \Delta\epsilon_j. \quad (25)$$

It can be seen that, besides configurations related to CT, the mean value of $\Psi_{f_1, \ldots, f_{N_e}}$ also contains contributions from configurations in which a valence electron is still attached to the Cs nucleus (therefore, they correspond to pure excitation of the cluster). Therefore, it is strictly an upper bound to the exact energy deposit given in Eq. (21). Both equations (23) and (24) are very easy to evaluate and the exact value of the energy deposit should be in between. At the low collision energies considered in this work, one can expect that CT of a single electron will dominate over all other processes. Therefore, the results obtained with these formulas should not be very different. As we will see below, this is the case in the present study.

The energy $E_{\mathrm{Li_{31}}^+}^*$ is the crucial quantity that is needed to evaluate the evaporation rates of different fragments. From these rates one can write master equations that describe the time evolution of the system after the collision (postcollisional evaporation). By solving these rate equations, one can predict the amount and size of the various evaporation fragments and evaluate the corresponding evaporation probabilities.

B. Evaporation rates and sequential evaporation model

The evaporation rates have been evaluated in the framework of the microscopic and microcanonical statistical model of Weisskopf. In this model, we evaluate the level density $\rho_N(E_N^*)$ of an N-particle cluster for a given internal excitation energy E_N^*. This level density has been evaluated from the specific entropy and internal energy (per atom) of bulk lithium. These properties can be easily derived from the known specific heat $c_p(T)$ at atmospheric pressure:

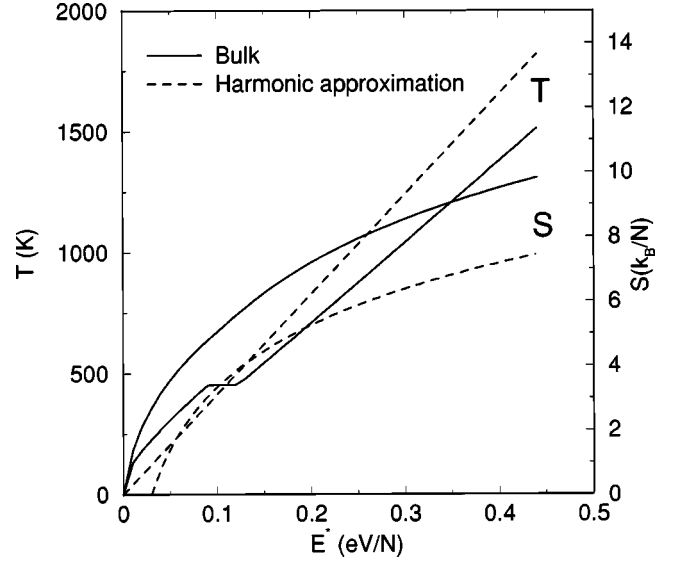$$s(T) = \int_0^T \frac{c_p(T')}{T'} dT', \quad (26)$$

FIG. 7. Temperature and entropy vs internal energy E_N^* for $\mathrm{Li_{31}}^{q+}$ clusters. Solid lines, curves obtained from the specific heat of bulk lithium [25]; dashed lines, harmonic approximation.

$$\varepsilon(T) \simeq h(T) - h_0 = \int_0^T c_p(T') dT', \quad (27)$$

where h_0 is the enthalpy at $T=0$. The thermodynamic relation $h = \varepsilon + Pv$, where v denotes the specific volume, allows us to identify the specific internal energy ε with h, since the term Pv up to the boiling point is very small.

We have used the experimental specific heat measured at a constant pressure of 1 atm given by Alcock *et al.* [25] in the temperature range from 0 K up to the normal boiling temperature $T_v = 1600$ K. With the help of Eqs. (26) and (27) the specific entropy and the temperature may be expressed as functions of the specific energy.

In the microcanonical ensemble, the number of states per unit energy, the level density $\rho_N^v(E_N^*)$, is related to the entropy $S(E_N^*) = Ns(\varepsilon)$ through the usual formula

$$k_B \ln[\rho_N^v(E_N^*)] = Ns(\varepsilon), \quad (28)$$

where $s(\varepsilon)$ is the specific entropy. The variation of the entropy $S = Ns$ and the temperature T with E_N^* is shown in Fig. 7. The figure also includes the curves obtained in the harmonic approximation. In this approximation the bulk is represented by a set of N quantum-mechanical harmonic oscillators. Thus, the difference with the experimental curves is the signature of anharmonic effects in bulk lithium. Notice that the latter effects are visible even at very low temperature.

Within the Weisskopf theory [26,27], the rate of evaporation of a monomer $k_{N,1}$ is given by

$$k_{N,1}(E_N^*) = \frac{g^{(1)}\mu_1}{\hbar^3\pi^2} \int_0^{E_N^* - D_{N,1}} \frac{\rho_{N-1}^v(E_N^* - e - D_{N,1})}{\rho_N^v(E_N^*)} \sigma(e) e \, de, \quad (29)$$

where $g^{(1)}$ is the spin degeneracy of the emitted monomer ($g^{(1)}=2$ for a lithium atom), e and μ_1 are the kinetic energy and the reduced mass of the monomer, respectively, and $D_{N,1}$ is the separation energy of a monomer from the parent cluster. σ is the fusion cross section for the product cluster and the monomer, and is taken to be πR_C^2 (classical approximation, i.e., an atom sticks when it hits a cluster), where $R_C = r_s N^{1/3}$ is the radius of the parent cluster ($r_s = 3.25$ a.u. for lithium). Equation (29) has been used to evaluate the rate constants in Sec. III. For dimer evaporation, the rate constant $k_{N,2}$ is given by

$$k_{N,2}(E_N^*)=\frac{g^{(2)}\mu_2}{\hbar^3\pi^2}\frac{1}{\hbar\omega_d}\int_0^\alpha dx\int_0^{E_N^*-D_{N,2}-x}$$

$$\times\frac{\rho_{N-2}^v(E_N^*-D_{N,2}-e-x)}{\rho_N^v(E_N^*)}\sigma(e)\,e\,de,\quad(30)$$

where

$$\alpha=\begin{cases}E_N^*-D_{N,2}, & E_N^*-D_{N,2}\lesssim D_{2,1}\\ D_{2,1}, & E_N^*-D_{N,2}>D_{2,1}.\end{cases}$$

$g^{(2)}$ is the spin degeneracy of the emitted dimer ($g^{(2)}=1$ for Li_2), μ_2 is its reduced mass, and ω_d is the angular frequency of the dimer Li_2 in a classical harmonic approximation ($\hbar\omega_d=0.0435$ eV, see Ref. [28]). As in Eq. (29), we have used $\sigma=\pi R_C^2$. The average kinetic energy of the ejected monomer and the kinetic and vibrational energies of the ejected dimer are obtained using a similar procedure (see Ref. [12]). The above formulas do not include contributions from the rotational degrees of freedom.

Integration of Eqs. (29) and (30) has been performed numerically using the level density obtained from the bulk entropy as given in Eq. (28). Recent experimental work with mass-selected free Na_N clusters ($N=70$–200) at constant temperature [29] has shown that the use of bulk quantities is a reasonable approximation. Indeed these experiments show that, with the exception of the region where the phase transition occurs (melting), the specific heat is almost independent of cluster size and close to its bulk value. Dissociation energies of the different Li_N^+ fragments have been taken from experiment [30].

When the energy deposit is larger than the dissociation energy of Li_{31}^+, the cluster can evaporate one or several atoms. Our model for evaporation has been described in detail in Ref. [12]. The model is based on the assumption that, in a single event, a cluster of arbitrary size N can only evaporate a monomer or a dimer. Therefore, fragments with less than $N-2$ atoms can only be produced by sequential emission of monomers or dimers. We have shown in Ref. [12] that this is a reasonable approximation because evaporation of large fragments is slower and requires more energy than evaporation of a small fragment. This is also confirmed by our results of Sec. V, which show that dimer production rates are much smaller than monomer production rates. Therefore, one can reasonably expect that the rates for production of trimers will be even smaller.

Time integration is performed up to $t=\tau_e$, the value of the experimental TOF. This leads to branching ratios for the different fragments and, hence, to partial cross sections. The partial evaporation probabilities are given by

$$P_{ev,j}(b)\equiv\frac{n_{N-j}(\tau_e)}{N^{(0)}},\quad(31)$$

where $N^{(0)}$ is the number of clusters of size N at $t-t_c=0$, i.e., just after the collision, and $n_{N-j}(\tau_e)$ is the number of clusters that have lost j atoms at $t-t_c=\tau_e$. The probabilities that are directly related to the experimental measurements are obtained by multiplying the charge-transfer probability $P^{6s\overline{6s}6p\overline{6p}\cdots}$ by the evaporation probabilities. Thus, the probability of finding a specific singly charged fragment i after charge transfer is defined as

$$P_{Li_{31-i}^+}(b)=P^{6s\overline{6s}6p\overline{6p}\cdots}(b)P_{ev,i}(b).\quad(32)$$

In all cases, the cross sections are evaluated by integration of the corresponding probabilities over impact parameter:

$$\sigma_\alpha=2\pi\int_{R_C}^\infty bP_\alpha(b)db.\quad(33)$$

The choice of the lower integration limit is consistent with the use of a jellium approximation which prevents from describing the collision dynamics below the cluster surface. This means that the calculated cross sections will be affected by an error that is proportional to the geometrical cross section of the cluster. As a rule of thumb, the error is approximately given by

$$\Delta\sigma_\alpha\simeq\tfrac{1}{2}\pi R_C^2 P_{\alpha,C},\quad(34)$$

where $P_{\alpha,C}$ is the mean value of the α transition probability in the neighborhood of the cluster surface. As discussed in Ref. [12], this is a good approximation when electronic transitions occur well outside the jellium surface.

V. COMPARISON BETWEEN THEORY AND EXPERIMENT

Figure 8 shows the charge-transfer probability as a function of impact parameter for an impact velocity of 0.024 a.u. It can be seen that the relevant transitions occur far beyond the cluster surface, in the region $b\simeq30$ a.u. As mentioned, this is a necessary condition for the validity of the theoretical model. We have checked that the general trends of the transition probability shown in Fig. 8 barely change with impact velocity; only a slight decrease in the absolute value has been observed.

Figure 9 shows the collisional energy deposit $\delta E_{Li_{31}^+}^*$ as a function of impact parameter. This energy deposit has been evaluated using the approximate equations (23) and (24), which are, respectively, lower and upper bounds to the exact energy deposit. It can be seen that the results obtained with both formulas are very similar, which supports the approximations that have been used to evaluate the energy deposit. The energy deposit exhibits strong oscillations as a function
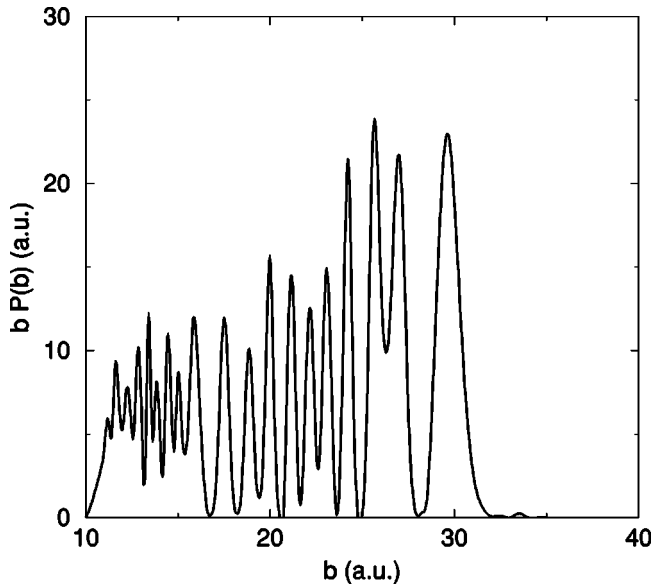
FIG. 8. Calculated charge-transfer probability P_{CT} times impact parameter as a function of impact parameter for $v = 0.024$ a.u.

of impact parameter. This is the result of the oscillatory behavior of the transition probabilities (see Fig. 8). This behavior is quite predictable, since the efficiency of the CT process (measured by the CT probabilities) imposes severe constraints on the energy that can be deposited. As for transition probabilities, the collisional energy deposit barely changes with impact energy: only a small decrease in absolute value is obtained when impact velocity increases. Now, experimentally, it is impossible to have access to the impact-parameter dependence of the energy deposit. Instead, as explained in Sec. III B, it has been possible to estimate an upper limit of around 1.9 eV. One can see in Fig. 9 that this value is compatible with the calculated energy deposit.
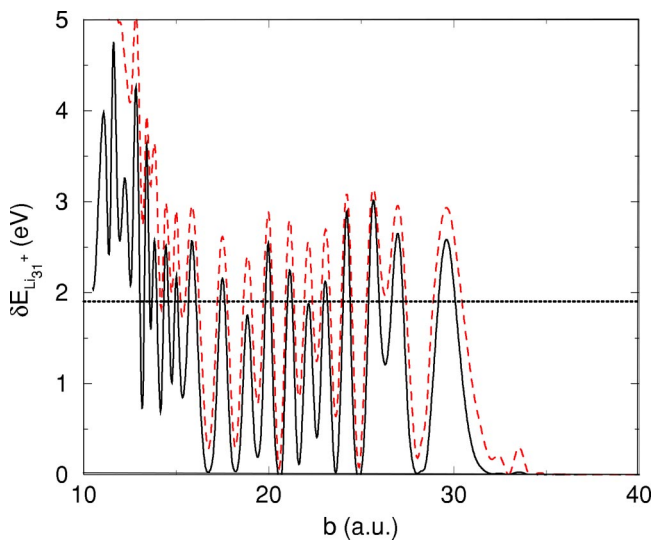

FIG. 9. Energy deposit as a function of impact parameter. Full line: results from Eq. (23). Dashed line: results from Eq. (24). The horizontal dotted line represents the experimental upper bound value.
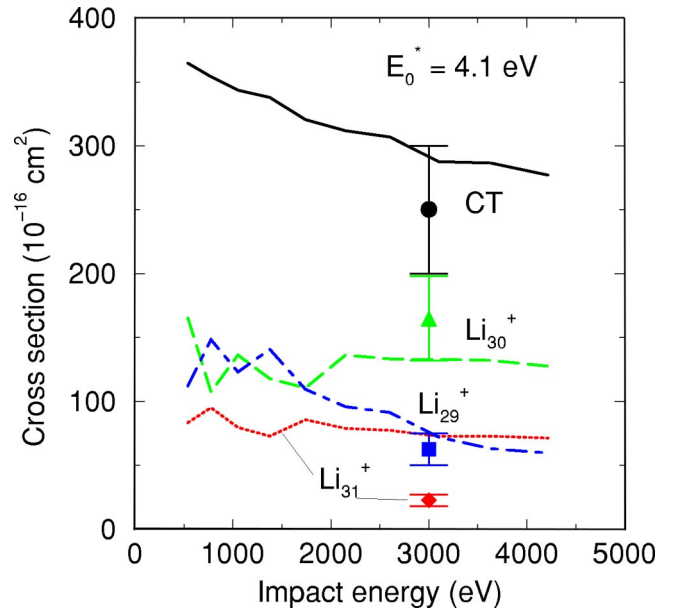

FIG. 10. CT and evaporation cross sections. Symbols with error bars, experiment (valid in the range 1–4 keV); lines, theory. CT, full line and circle; Li_{31}^{+}, dotted line and diamond; Li_{30}^{+}, dashed line and triangle; Li_{29}^{+}, dot-dashed line and square.

We have also checked that, for the largest values of the energy deposit given in Fig. 9, the evaporation time is never smaller than 10^{-10} s. Therefore it is never smaller than the typical vibrational periods of the cluster ($\simeq 10^{-12}$ s), which is consistent with the use of a statistical model to evaluate evaporation rates.

In view of the similarity of the two curves shown in Fig. 9, we have only used the energy deposit obtained from Eq. (23) to evaluate fragmentation cross sections. As explained in Sec. III (see also Ref. [15]), for a meaningful comparison between theory and experiment, one has to include the effect of the initial cluster energy. In Fig. 10 we compare the total and partial CT cross sections obtained from the theoretical model described in Sec. IV with those determined experimentally. The theoretical partial cross sections have been evaluated for an initial cluster energy of $E_0^* = 4.1$ eV, which is within the evaporative ensemble energy distributions shown in Figs. 3(b) and 3(c), and $\tau_e = 3$ μs (approximately the TOF in the present experiment). Figure 10 shows a reasonable agreement between theory and experiment. In particular, the theoretical results confirm that the dominant fragment is Li_{30}^{+}, followed by Li_{29}^{+} and Li_{31}^{+} in almost similar proportions. The results shown in Fig. 10 slightly improve on those reported in Ref. [15] because in this work the energy deposit has been evaluated using a larger number of excited cluster states.

Obviously, the choice of different values of E_0^* and τ_e is irrelevant for the total CT cross section. However it has dramatic consequences on the fragmentation ratios. In Ref. [15] we have shown a few examples of how these ratios change when E_0^* and τ_e are varied. These examples have led us to conclude that good agreement between theory and experiment is only possible by using the experimental value of the
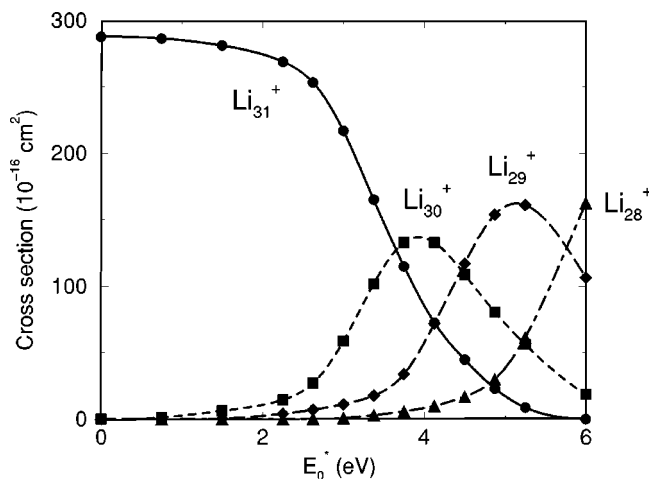
FIG. 11. Evaporation cross sections as functions of initial energy for $v = 0.024$ a.u.

TOF and a cluster temperature consistent with the experimental distribution. Small deviations from this choice lead to enormous differences in fragmentation ratios and, therefore, to very different physical interpretations. Similarly, any deficiency in the theoretical treatment may lead to results in complete disagreement with experiment. For instance, we have checked that exclusion of the collisional energy deposit always leads to Li_{31}^+ as the dominant species, in strong disagreement with experiment.

Now, as mentioned in Sec. III, cluster projectiles produced in the experiment constitute an evaporative ensemble. Furthermore, as explained in Secs. II and III, besides Li_{31}^{2+} clusters, there is a significant proportion of Li_{30}^{2+} clusters that enter the collision cell at $t = t_c$. Although the CT cross sections for both clusters are expected to be the same [and, in fact, this has been used to deduce the experimental value of the CT cross section from Eq. (6)], this is not the case for the initial energy distributions shown in Fig. 3. This figure shows that Li_{30}^{2+} clusters are produced with less initial energy than Li_{31}^{2+} clusters, because the former are the result of a UD process that absorbs part of the initial energy. All these factors must be taken into account for a more rigorous comparison between theory and experiment.

To this aim, we have evaluated the partial cross sections for different values of the initial energy at an impact velocity of 0.024 a.u. ($\simeq 3$ keV). The results are shown in Fig. 11. We must note that the energy in abscissas is just the initial cluster energy, while the cross sections have been evaluated by including both this initial energy and the collision energy deposit shown in Fig. 9 (the latter depends on impact parameter). It can be seen in Fig. 11 that Li_{30}^+ is the dominant species when the initial internal energy of the Li_{31}^{2+} cluster lies approximately around 4 eV. In order to compare with experiment one should convolute these cross sections (and those corresponding to CT from Li_{30}^{2+}) with the energy distributions given in Fig. 3. The latter figure shows that the energy distribution of Li_{31}^{2+} clusters peaks around 5 eV (i.e., ~1 eV higher in energy than in Fig. 11), which would lead to Li_{29}^+ as the dominant fragment instead of to Li_{30}^+ as

observed experimentally. This cannot be considered as a significant discrepancy between theory and experiment because fragmentation rate constants are extremely sensitive to the internal energy of the cluster. For example, Fig. 11 shows that a small variation of 0.2–0.3 eV may lead to significant variations in these ratios. In fact, we have checked that by only shifting 0.8 eV down in energy the cross sections shown in Fig. 11, convolution with the energy distribution given in Fig. 3(b) leads to cross sections of 44.4 Å^2 for Li_{31}^+, 144.0 Å^2 for Li_{30}^+, 86.7 Å^2 for Li_{29}^+, and 18.8 Å^2 for Li_{28}^+ and smaller fragments, which agree reasonably well with the experimental values (even better than those obtained by using a single value of the initial cluster energy; see Fig. 10). Errors of this size in δE may come from the region of impact parameters near or below the cluster surface, where the use of the spherical jellium approximation prevents one to obtain any quantitative information. As we have seen, this error barely affects the calculated CT cross sections because CT occurs at large impact parameters and this is the region that contributes most to the cross section. However it is difficult to know its effect on the energy deposit because the latter oscillates with almost constant amplitude for all impact parameters.

Another aspect that remains uncertain is the accuracy of a dynamical approach that makes use of virtual (unoccupied) orbitals arising from density-functional theory. This approximation is common usage in many areas of cluster physics and solid-state physics, especially in the context of dynamical treatments. The good agreement found between experiment and theory for the absolute value of the CT cross section (not only in this case, but also in the case of Na_9^+ +Cs collisions) clearly supports the use of virtual orbitals for this purpose, but it remains to be proved that they are good enough to provide energy deposits within a 0.2–0.3 eV accuracy.

Finally, one has to keep in mind that, in the experiment, the collision cell is reached by two doubly charged species, Li_{31}^{2+} and Li_{30}^{2+}, while the theoretical simulations have only been performed for Li_{31}^{2+} projectiles. Although the absolute CT cross section is practically identical for both projectiles, it is not clear that the collisional energy deposit is also identical. To know this, one should perform a theoretical treatment of the Li_{30}^{2+} +Cs collision similar to that presented for the Li_{31}^{2+} +Cs collision, which is beyond the scope of the present work.

VI. CONCLUSION

We have presented a combined theoretical and experimental study of charge transfer and evaporation in collisions of slow Li_{31}^{2+} clusters with Cs atoms. The measured absolute charge-transfer cross sections are in excellent agreement with the theoretical values. We have shown the importance of including the experimental TOF and initial cluster energy (temperature) in the theoretical modeling. Indeed, the calculated fragmentation ratios are only in good agreement with experiment when (a) time integration of the rate equations is performed up to the experimental TOF, and (b) the initial

cluster energy is compatible with the energy distribution of the evaporative ensemble produced in the experiment. This agreement supports the physical assumptions of our model, in particular, the separation between CT and evaporation, which is justified by the different time scales associated with these processes. Although some discrepancies between theory and experiment still remain when the calculated evaporation cross sections are convoluted with the initial energy distribution of Li_{31}^{2+} clusters, we can conclude unambiguously that the observed fragmentation patterns can only be reproduced if CT is accompanied by an energy deposit that does not exceed 1.9 eV.

[1] C. Bréchignac, Ph. Cahuzac, J. Leygnier, R. Pflaum, and J. Weiner, Phys. Rev. Lett. **61**, 314 (1988).

[2] U. Saalmann and R. Schmidt, Phys. Rev. Lett. **80**, 3213 (1998).

[3] M. Barat, J.C. Brenot, H. Dunet, J.A. Fayeton, and Y.J. Picard, J. Chem. Phys. **114**, 179 (2001).

[4] P. Blaise, S.A. Blundell, C. Guet, and R.R. Zope, Phys. Rev. Lett. **87**, 063401 (2001).

[5] D. Babikov, E.A. Gislason, M. Sizun, F. Aguillon, and V. Sidis, J. Chem. Phys. **112**, 7032 (2000).

[6] F. Calvayrac, P.-G. Reinhard, E. Suraud, and C.A. Ullrich, Phys. Rep. **337**, 493 (2000).

[7] M.F. Politis, P.A. Hervieux, J. Hanssen, M.E. Madjet, and F. Martín, Phys. Rev. A **58**, 367 (1998).

[8] C. Bréchignac, Ph. Cahuzac, B. Concina, J. Leygnier, and I. Tignères, Eur. Phys. J. D **12**, 185 (2000).

[9] O. Knospe, J. Jellinek, U. Saalmann, and R. Schmidt, Eur. Phys. J. D **5**, 1 (1999).

[10] O. Knospe, J. Jellinek, U. Saalmann, and R. Schmidt, Phys. Rev. A **61**, 022715 (2000).

[11] B. Zarour, J. Hanssen, P.A. Hervieux, M.F. Politis, and F. Martín, J. Phys. B **33**, L707 (2000).

[12] P.A. Hervieux, B. Zarour, J. Hanssen, M.F. Politis, and F. Martín, J. Phys. B **34**, 3331 (2001).

[13] C. Bréchignac, Ph. Cahuzac, J. Leygnier, and J. Weiner, J. Chem. Phys. **101**, 6992 (1994).

[14] C. Klots, J. Chem. Phys. **83**, 5854 (1985); Z. Phys. D: At., Mol. Clusters **5**, 83 (1987).

[15] C. Bréchignac, Ph. Cahuzac, B. Concina, J. Leygnier, L.F. Ruiz, B. Zarour, P.A. Hervieux, J. Hanssen, M.F. Politis, and F. Martín, Phys. Rev. Lett. **89**, 183402 (2002).

[16] C. Bréchignac, Ph. Cahuzac, F. Carlier, and M. Frutos, Phys. Rev. B **49**, 2825 (1994).

[17] J. Perel and H.L. Daley, in *Electronic and Atomic Collisions*, edited by B.C. Cobic and M.V. Kurepa (Institute of Physics, Beograd, Yugoslavia, 1973), Vol. II.

[18] C. Bréchignac, Ph. Cahuzac, B. Concina, and J. Leygnier, Eur. Phys. J. D **16**, 91 (2001).

[19] H. Bachau, P. Galan, and F. Martín, Phys. Rev. A **41**, 3534 (1990).

[20] M. Brack, Rev. Mod. Phys. **65**, 677 (1993).

[21] F. Calvo and F. Spiegelmann, J. Chem. Phys. **112**, 2888 (2000).

[22] F. Calvo and F. Spiegelmann, Phys. Rev. Lett. **89**, 266401 (2002).

[23] C.A. Ullrich, P.G. Reinhard, and E. Suraud, Phys. Rev. A **62**, 053202 (2000).

[24] H. Lüdde and R.M. Dreizler, J. Phys. B **18**, 107 (1985).

[25] C.B. Alcock *et al.*, J. Phys. Chem. Ref. Data **23**, 385 (1994).

[26] V. Weisskopf, Phys. Rev. **52**, 295 (1937).

[27] P.A. Hervieux and D.H.E. Gross, Z. Phys. D: At., Mol. Clusters **33**, 295 (1995); D.H.E. Gross, Phys. Rep. **279**, 119 (1997).

[28] K.P. Huber and G. Herzberg, *Molecular Spectra and Molecular Structure* (Van Nostrand, Princeton, 1979), Vol. 4.

[29] M. Schmidt *et al.*, Nature (London) **393**, 238 (1998).

[30] C. Bréchignac, H. Busch, Ph. Cahuzac, and J. Leygnier, J. Chem. Phys. **101**, 6992 (1994).